
MiniCPM: Unveiling the Potential of Small Language Models with Scalable Training Strategies

XXX *

Tsinghua University

Abstract

In this context, we introduce MiniCPM, specifically the 1.2B and 2.4B non-embedding parameter variants, not only excel in their respective categories but also demonstrate capabilities on par with 7B-13B LLMs. Regarding model scaling, we employ extensive model wind tunnel experiments for stable and optimal scaling. For data scaling, we introduce a Warmup-Stable-Decay (WSD) learning rate scheduler (LRS), conducive to continuous training and domain adaptation. With WSD LRS, we are now able to efficiently study data-model scaling law without extensive retraining experiments on both axes of model and data, from which we derive the much higher compute optimal data-model ratio than Chinchilla Optimal. MiniCPM models are available publicly ¹.

1 Introduction

Recently, a resurgence of interest has been observed in the domain of SLMs, evidenced by the advent of a series of innovative models such as the Phi series (Gunasekar et al., 2023; Li et al., 2023b; Javaheripi & Bubeck, 2023), TinyLlama (Zhang et al., 2024a), MobileLLM (Liu et al., 2024), and Gemma (Banks & Warkentin, 2024), among others.

In this paper, we introduce MiniCPM, a series of SLMs, which primarily builds on two models, endowed with 2.4B and 1.2B non-embedding parameters respectively, and they rank preeminently in their respective 2B and 1B scale categories. MiniCPM also exhibits comparable capabilities to those of 7B~13B language models, such as Llama2-7B (Touvron et al., 2023), Mistral-7B (Jiang et al., 2023), Gemma-7B (Banks & Warkentin, 2024), and Llama-13B (Touvron et al., 2023), etc. This is exemplified through our model wind tunnel experiments that encompass comprehensive hyper-parameter optimization (Section 3), and the deployment of a WSD (Warmup-Stable-Decay) learning rate scheduler (Section 4). The latter is tailored for continuous training with an un-predefined pre-training token number and makes the reusing of model intermediate checkpoints highly feasible. With the WSD scheduler, we are now also capable of studying the data-model scaling law with linear effort on the model axis and a negligible effort on the data axis, while the traditional ones need quadratic effort considering the scaling along both model and data axes. The result of the scaling law indicates a much higher data size/model size ratio compared with Chinchilla Optimal (Hoffmann et al., 2022).

2 Related Work

Small Language Models. Notable examples within the current landscape of SLMs include the Phi series (Gunasekar et al., 2023; Li et al., 2023b; Javaheripi & Bubeck, 2023), TinyLlama (Zhang et al., 2024a), MobileLLM (Liu et al., 2024), and Gemma (Banks & Warkentin, 2024), etc. A variety of methodologies have been explored to augment the efficacy of SLMs. These include the incorporation of high-quality data (Gunasekar et al., 2023; Li et al., 2023b; Javaheripi & Bubeck, 2023), the application of structure pruning techniques (Xia et al., 2023), and the reconfiguration of model architectures (Liu et al., 2024), among others.

*The original paper is located at <https://arxiv.org/abs/2404.06395>. This version has been modified by LuYF-Lemon-love <luyanfeng_nlp@qq.com> for personal study.

¹<https://github.com/OpenBMB/MiniCPM>

Scalable Pre-training Strategies. Since the discovery of scaling law (Kaplan et al., 2020; Rae et al., 2021; Aghajanyan et al., 2023), scientifically and predictably (Achiam et al., 2023; Hu et al., 2023; Du et al., 2024) scaling up the LLMs has been pursued from diverse perspectives, especially for the pre-training stage. In terms of training stability, the Tensor Program series (Yang et al., 2022; 2023) is introduced to ensure optimal hyper-parameter consistency across varying model scales, a technique employed in training CerebrasGPT (Dey et al., 2023). Furthermore, Wortsman et al. (2023) suggest leveraging smaller models to anticipate and mitigate instabilities in larger model training. From the training data standpoint, various data-centric strategies have been advocated (Xie et al., 2024; Shi et al., 2023; Ye et al., 2024). In the realm of training methodologies, prior research has delved into diverse learning rate schedulers (LRS) (Howard & Ruder, 2018; Raffel et al., 2020; Hundt et al., 2019), with the Cosine LRS (Loshchilov & Hutter, 2016) emerging as the predominant choice in LLMs. Kaplan et al. (2020) and Hoffmann et al. (2022) have meticulously examined the hyper-parameters of Cosine LRS, thereby laying a foundational groundwork for subsequent pre-training works. Of these, DeepSeek (Bi et al., 2024) bears the closest resemblance to our proposed WSD LRS. Concerning batch size scheduling, Smith et al. (2017) advocates for incrementing batch size as an alternative to diminishing learning rate, a strategy recently adopted by Yi-9B (Young et al., 2024).

3 Model Wind Tunnel Experiments

3.1 Scaling Hyper-parameters Invariant LM

Tensor Program (Yang et al., 2022; 2023) proposes a framework to stabilize the hyper-parameters for models with different scales. The main part of the Tensor Program is the width scaling (Yang et al., 2022) and the depth scaling (Yang et al., 2023). The former technique supports CerebrasGPT (Dey et al., 2023) to predict the loss of LLMs more accurately. In MiniCPM, we use both two scaling techniques. The specific scaling operations are listed in Table 1. We do not apply the attention softmax scaling techniques (Yang et al., 2022). Despite Yang et al. (2023) observing that depth scaling for a network with block depth larger than two is not satisfying, we find the resulting optimal learning rate is stable empirically.

Name	Specific Operation
Embedding Output Scaling	Multiply the output of the embedding by $scale_emb$
Residual Connection Scaling	Scale the output tensor of a block before adding to each residual connection in each layer by $scale_depth / \sqrt{\text{num_layers}}$
Initialization of Tensors	Set the initialization standard deviation of each two-dimensional tensor parameter to $init_std / \sqrt{d_m / d_{base}}$, and set other parameters' initialization to 0.1
Learning Rate Scaling of Tensors	Adjust the learning rate of each two-dimensional tensor parameter to $1 / (d_m / d_{base})$ times the learning rate of other parts (or the overall learning rate)
LM Head Scaling	Adjust the output logits to $1 / (d_m / d_{base})$ times the original value

Table 1: List of operations used when applying tensor program techniques.

3.2 Optimal Batch Size

We follow Kaplan et al. (2020) to determine the batchsize from expected loss, with a slight modification from their setting. We conduct experiments on 0.009B, 0.03B, and 0.17B models, respectively, toward this goal. Each model size is trained on 6 batch sizes with a global learning rate of 0.01 and cosine learning rate scheduler. We observe the trend of the optimal batch size with loss on the C4 (Raffel et al., 2019) dataset (red line in the Figure 1).

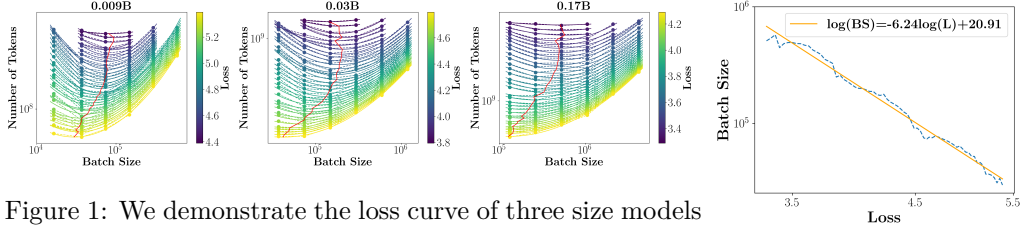


Figure 1: We demonstrate the loss curve of three size models trained using different batch sizes. Each vertical line formed by points with a gradient color represents a training curve. Lighter colors denote higher loss.

Figure 2: The connected optimal batch sizes.

As shown in Figure 1, we plot the batch size in the x-axis, and token consumption in the y-axis, the color of the points represents a loss. Thus a horizontal line formed by the color points denotes a training curve. we use parabolas to fit the equal-loss points and connect the minima of the parabolas with red lines. The lines demonstrate the optimal batch size shifts large as the loss decreases. We then connect the three lines (see Figure 2) and find that the lines connect each other well into a linear relationship in the log space, from which we obtain the following relationship between batch size bs and C4 Loss L : $bs = \frac{1.21 \times 10^9}{L^{6.24}}$. We note that it might seem strange that the batch size should be estimated from a rough loss prediction that we can only have after training.

3.3 Optimal Learning Rate

Due to our use of Tensor Program (Yang et al., 2022; 2023), we anticipate that the learning rate, will not undergo significant changes during model scaling. In Figure 3, we find that although the model size has increased by ten times, the optimal base learning rate ² does not show a noticeable shift and remains around 0.01.

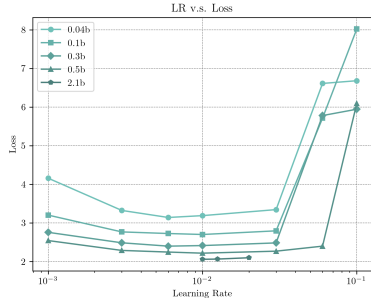


Figure 3: Loss vs Learning Rate. After applying for the Tensor Program, the learning rate shift becomes minimal.

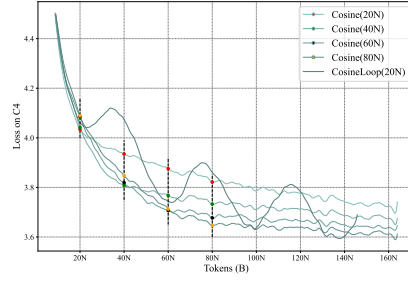


Figure 4: Cosine Learning Rate Scheduler with different periods. The Y-axis is the loss on the C4 corpus.

4 WSD Learning Rate Scheduler

4.1 Analysing Cosine LRS

The current commonly used learning rate strategy is the Cosine LRS (Kaplan et al., 2020; Hoffmann et al., 2022; Rae et al., 2021; Touvron et al., 2023; Bai et al., 2023; Almazrouei et al., 2023), which gradually decreases the learning rate following a cosine curve after it reaches its maximum after the warmup stage.

A key hyper-parameter in the Cosine LRS is the step T at which Cosine decreases to the minimum for the first time. Typically, T is set to the total training step S for training

²The actual learning rate of 2-D tensors will be scaled according to Tensor Program.

with a predefined training step. Generally, it is believed that the learning rate should be high to enable sufficient exploration. We try *Cosine*(T) and *CosineLoop*(T) LRS, following the formula shown in Appendix B.1. The result can be seen in Figure 4. We can see that when the training step is $S = 20N, 40N, 60N, 80N$, the lowest loss is always achieved by the *Cosine*(T) where $T = S$. Both $T < S$ and $T > S$ are not optimal.

We hypothesize that the Cosine LR performs exceptionally well when $T = S$ because of the following two reasons:

- (1) Cosine LRS with $T = S$ has a longer duration of *high learning rate* training compared to $T < S$ and other LRS such as Linear LRS. This high learning rate might help the model find a better global optimum.
- (2) Cosine LRS with $T = S$ has a more thorough learning rate decay phase compared to Cosine LRS with $T > S$ and Constant LRS. This learning rate decay may involve unique training dynamics that enable the model to find a better local optimum.

4.2 WSD LRS

In light of the above perspective, we propose to explicitly divide the training stage into the high learning rate stage and learning rate decay stage. We name it as the Warmup-Stable-Decay (WSD) LRS. Especially, the WSD LRS contains three stages: the warmup stage (whose end step is denoted by W), the stable training stage (whose end step is denoted by T), and the remaining decay stage. The function form of WSD is:

$$WSD(T;s) = \begin{cases} \frac{s}{W}\eta, & s < W \\ \eta, & W < s < T \\ f(s-T)\eta, & T < s < S \end{cases} \quad (1)$$

where $0 < f(s-T) \leq 1$ is a decreasing function about s , η is the maximum learning rate.

4.3 Experiments

Loss Decreases Dramatically in Decay Stage. As shown in Figure 5, in the decay stage, as the learning rate begins to decrease, the loss experiences a significant rapid decline and quickly decreases to be equal to or lower than the Cosine LRS at step $T = S$. At the same time, we can reuse the model before decay and continue training with the previous high learning rate. After more steps of training S' , we can also perform annealing to achieve the same loss as the Cosine LRS at *Cosine*(S'). This verifies our assumption that the training stage can be explicitly split into the stable training and decay stages.

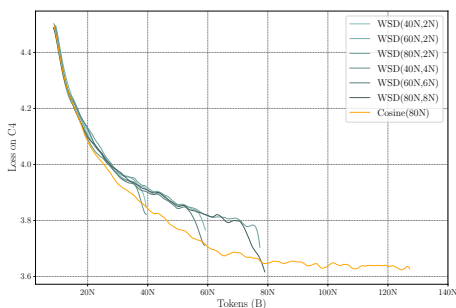


Figure 5: Model training loss has a sudden decrease in the decay stage of WSD LRS.

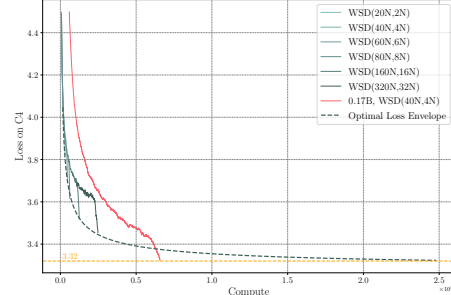


Figure 6: Continuous training a 0.036B model can match the performance of 0.17B model with an acceptable increase in training compute.

10% Steps are Enough. From the two-stage training perspective, shortening the decay stage will greatly benefit the fast test of different model checkpoints of stable training. Also shown in Figure 5, among all three stable training checkpoints in 40N, 60N, and 80N training data, having a decay of 10% of the total tokens is sufficient to achieve the best results, while a decay of 2.5% of total tokens falls short. Therefore, in the subsequent training experiments, we use a decay of about 10% to ensure full convergence.

Effective Data Scaling with WSD LRS. With WSD LRS, we can continuously train the LM to extreme convergence. In Figure 6, the green lines represent 0.036B models trained with different stable training tokens. Despite the last point of the 0.036B series being trained with many more tokens than Chinchilla Optimal (Hoffmann et al., 2022), it still has space for performance improvement.

By optimal performance, we mean the loss of training token D is achieved by $WSD(D, 0.1D)$. With a series of D , the losses will form the optimal loss envelope. Due to uncertainty about the function form of the loss envelope, we try two fitting formulas: (1) exponential: $L(C) = \alpha e^{-\beta C} + L_0$ and (2) power-law: $L(C) = \beta C^{-\alpha} + L_0$. We find that the power-law form fits better (similar to the Cosine LRS (Kaplan et al., 2020)). In Figure 6, the fitted curve is shown in green dotted lines.

To intuitively estimate and comprehend the effect of continuous training such a fixed-sized model, we also trained a 0.17B model with $WSD(40N, 4N)$, which is shown in pink in Figure 6. We can see that a 0.036B model can match the performance of a 0.17B model with an acceptable increase (~ 4 times) in training compute while saving a lot of inference computation (Sardana & Frankle, 2023) (saving ~ 5 times per inference call), indicating a better inference-compute-optimal setting (Sardana & Frankle, 2023).

4.4 Analysis of the Decay Stage

We calculate the maximum weight element update $\max_{ij}(W_{ij}^{(t+1)} - W_{ij}^{(t)})$ across all weight matrices in the MiniCPM-2.4B (Introduced in Section 6.1). As depicted in Figure 7, the updates exhibit a robust correlation with the learning rate's magnitude. This observation may not be trivial: the model checkpoints experience significant updates preceding the learning rate's decay, yet the loss exhibits minimal reduction. Conversely, during the decay stage, despite less pronounced weight alterations, there is an accelerated decrease in loss.

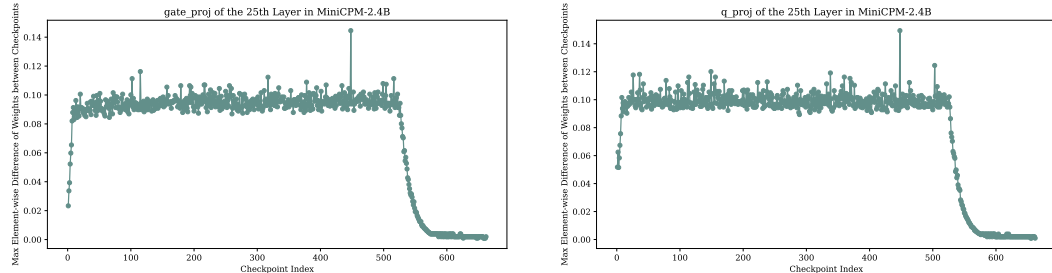


Figure 7: Max Difference of Checkpoints.

Further examination of the gradient data is undertaken by training a 0.2B model, meticulously recording every step gradient information, and evaluating the differences between consecutive steps, thereby providing an approximation of second-order gradient information.

We treat the gradient at step t as a flattened vector $\mathbf{g}^{(t)}$, and the parameter (also flattened as a vector $\mathbf{x}^{(t)}$) update between step t and $t + 1$ is $\mathbf{v}^{(t)} = \mathbf{x}^{(t+1)} - \mathbf{x}^{(t)}$. The gradient norm take the L2 norm of the gradient $\|\mathbf{g}^{(t)}\|$, gradient inner product is $\mathbf{g}^{(t+1)} \cdot \mathbf{g}^{(t)}$, the cosine of the gradient's angle is given by $\frac{\mathbf{g}^{(t+1)} \cdot \mathbf{g}^{(t)}}{\|\mathbf{g}^{(t+1)}\| \|\mathbf{g}^{(t)}\|}$.

Imaging the optimization process as a trajectory over a high-dimension manifold, first order directional derivative along the trajectory is computed as $D_1 = \frac{\mathbf{g}^{(t+1)} \cdot \mathbf{v}^{(t)}}{\|\mathbf{v}^{(t)}\|}$, and the second order directional derivative is $D_2 = \frac{(\mathbf{g}^{(t+1)} - \mathbf{g}^{(t)}) \cdot \mathbf{v}^{(t)}}{\|\mathbf{v}^{(t)}\|^2}$. D_1, D_2 enables an approximate estimation of the loss curvature on the trajectory, $K = \frac{|D_2|}{(1+D_1^2)^{\frac{3}{2}}}$. The results of these statistics over time are shown in Figure 8.

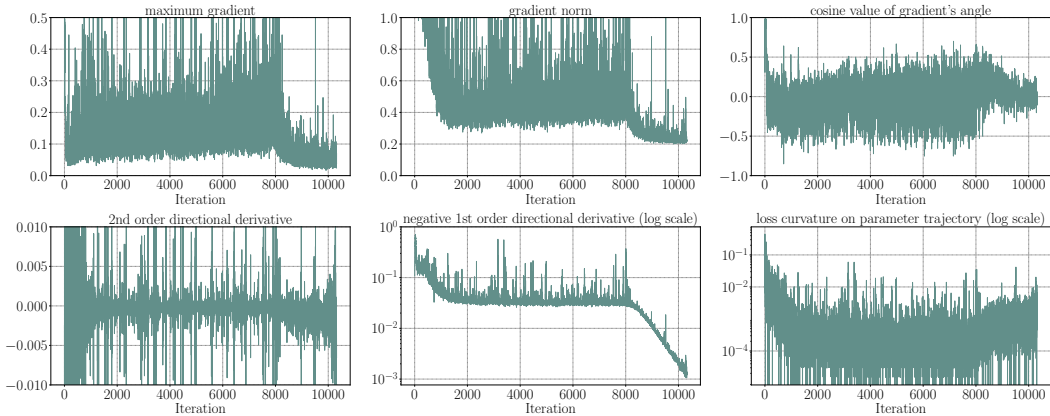


Figure 8: Gradient statistics over the training of a 0.2B model using WSD LRS. The exponential decay stage begins at 8000 steps.

We can see that the gradient norm diminishes during the decay phase, and upon commencement of this stage, the cosine between gradients predominantly assumes positive values, suggesting that in the decay phase, model parameters undergo consistent changes across steps. The curvature of the loss function also increases by a magnitude, indicating the proximity to a local optimum.

4.5 Measuring the Scaling Law with WSD LRS

Since the WSD scheduler has the advantage of arriving at the optimal loss of Cosine LRS after decaying from stable stage checkpoints of any step, we are now able to precisely measure the optimal scaling properties without re-training the models from scratch to different amounts of tokens, thus making the scaling law measurement much more efficient along the data axis.

We measure the scaling law along the data and model axes by training SLMs of 6 sizes ranging from 0.04B to 2B, each with 6 decayed models starting from the checkpoint of $10N$ to $60N$ data during the stable training stage. The final loss of each pair of data size and model size is shown in the blue lines in Figure 9.

Then we fit the losses with model size N and data size D following Hoffmann et al. (2022) using `scipy curvefit` function:

$$L(N, D) = C_N N^{-\alpha} + C_D D^{-\beta} + L_0 \quad (2)$$

The fitted curve along the data axis for each dataset and each checkpoint are shown in orange lines in Figure 9. Then we have the optimal model size N_{opt} , dataset size D_{opt} , given a fixed amount of compute $C = 6ND$ (Rae et al., 2021) as:

$$\frac{N_{opt}}{D_{opt}} = K^2 \left(\frac{C}{6} \right)^{\eta}, \quad (3)$$

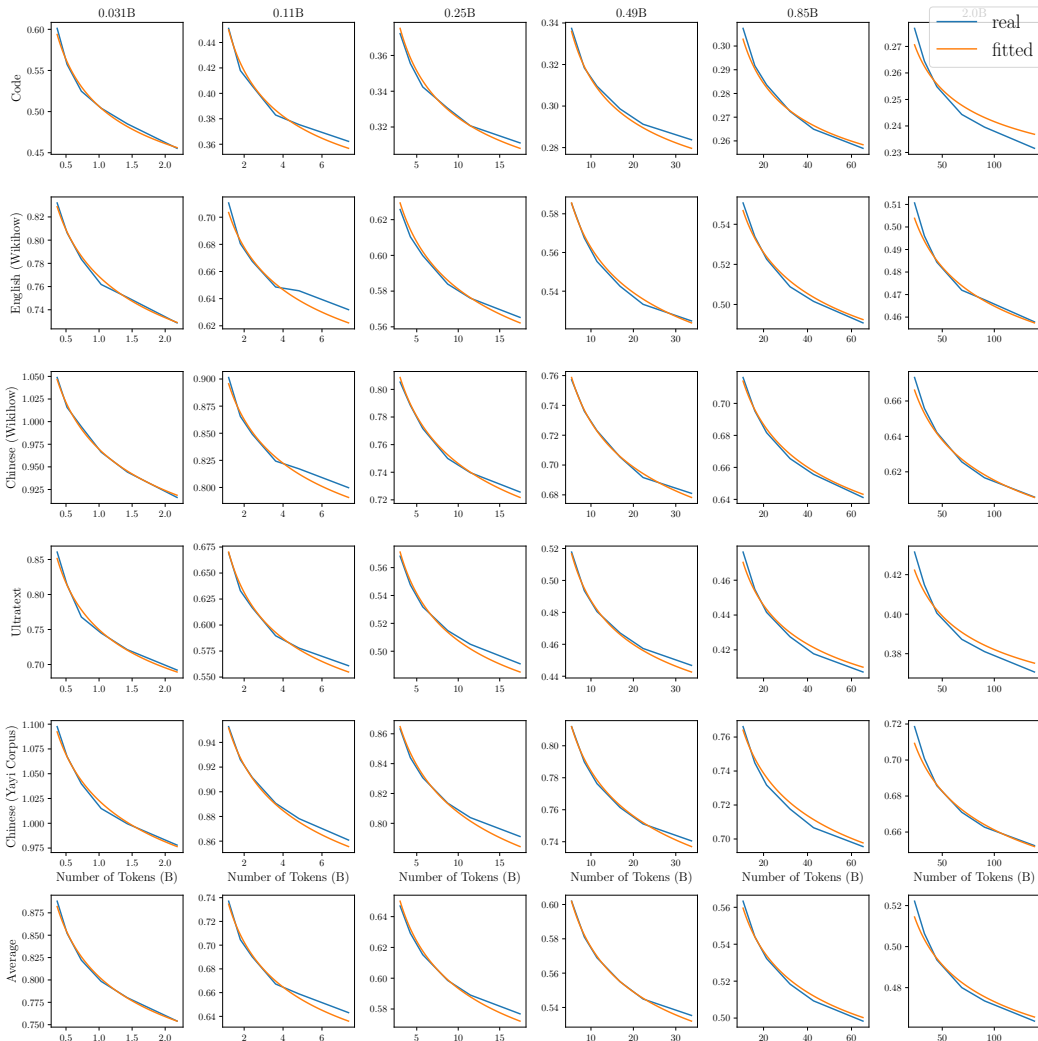


Figure 9: The fitted scaling law plotted along the data amount axis for each model and each task. The fitted result is satisfying except for the last checkpoints of the 0.11B and 0.25B model.

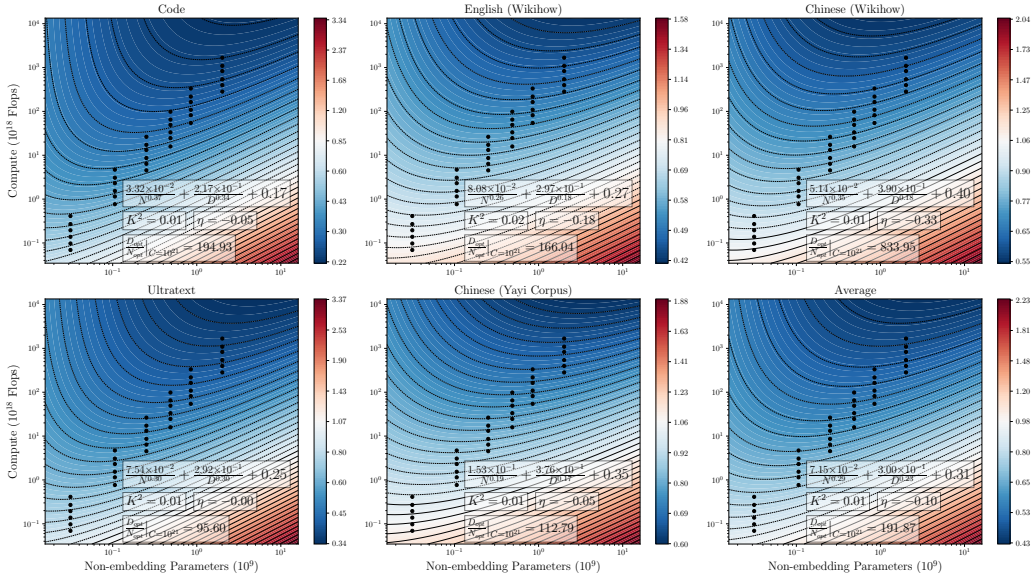


Figure 10: The fit result of the scaling experiment with WSD Scheduler. The black dots in a horizontal line denote the decayed checkpoints in different compute within the same model size.

where $K = \left(\frac{\alpha C_N}{\beta C_D}\right)^{\frac{1}{\alpha+\beta}}$, and $\eta = \frac{\beta-\alpha}{\alpha+\beta}$. From Equation 3, when $\alpha = \beta$, N_{opt}/D_{opt} is a constant, supporting Hoffmann et al. (2022)'s claim, and when $\alpha < \beta$, we should emphasize more on parameter scaling (Kaplan et al., 2020), and vice versa.

In our experiments, the fitted relationship between loss and N, D is shown in the contour plot of equal loss in Figure 10. We can see that in all evaluation corpora, we have $\beta < \alpha$. More specifically, on average, we have $\alpha = 0.29, \beta = 0.23, K^2 = 0.01, \eta = -0.10$. Since α is slightly larger than β , this result shows that as the computation scale, we should slightly emphasize more on data scaling than model scaling, which aligns with Hoffmann et al. (2022).

A larger data-to-model ratio means that we can absorb more data into a smaller model than we previously thought, which is more efficient for inference and deployment.

5 Two Stage Pre-training Strategy

In light of the pronounced loss decrease observed during the decay stage of the WSD LRS, we postulate that the integration of high-quality labeled data in this phase presents dual advantages:

- Introducing this data during the annealing phase, in addition to the SFT stage, fosters a more comprehensive model learning. Specifically, it facilitates a more pronounced loss reduction in relation to the SFT data distribution, rather than the pre-training data distribution.
- In contrast to a uniform distribution of high-quality data throughout the entire pre-training process, this method enhances training by concentrating on data and sustaining continuous pre-training. If we do not predetermine a training step, we will repeat a small dataset throughout an ongoing pre-training process, which could lead to negative effects.

Based on these two hypotheses, we propose the following training strategy:

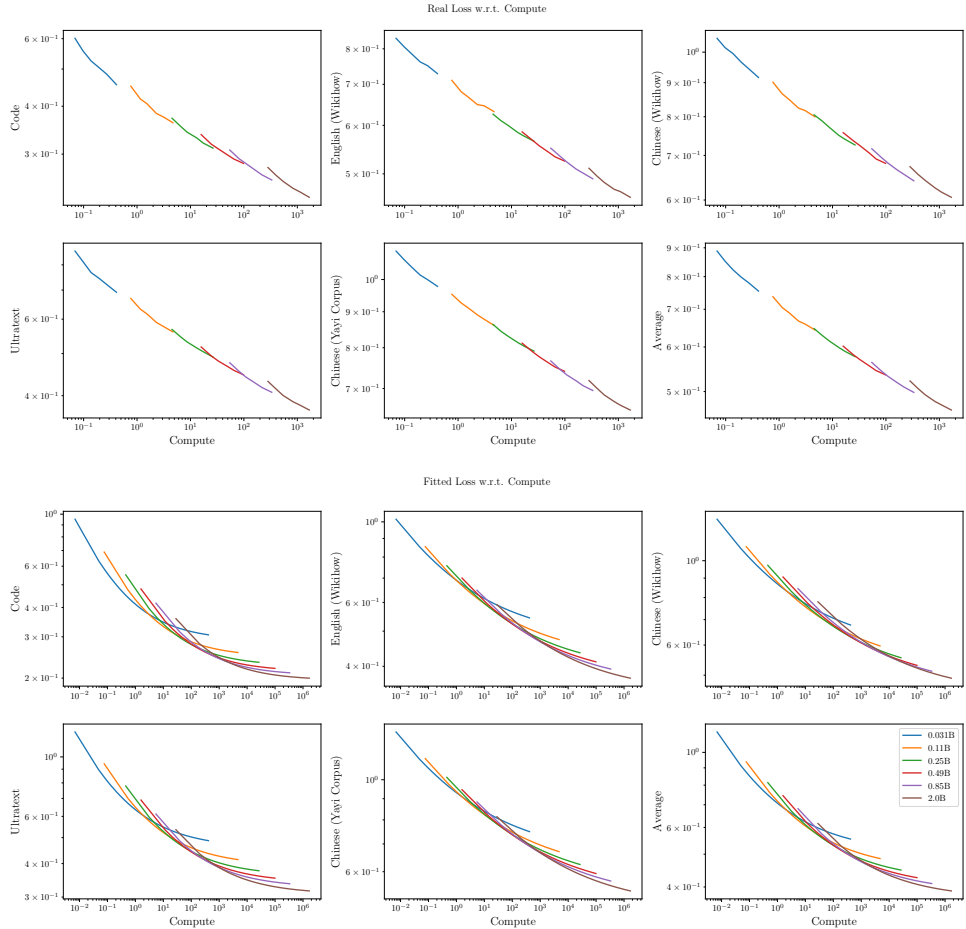


Figure 11: The result of scaling experiments with WSD Scheduler (above) and the fitted scaling curve (below). The x-axis is the computation Flops $C = 6ND$, each color of the line represents the same model with different computation Flops. We can see that smaller models are better than larger models when the Flops are small and worse when the Flops are large. Thus models of different sizes will intersect with each other in the plot around the compute optimal regime.

- During the pre-training phase, only use large-scale coarse-quality pre-training data, which is abundant and can support continuous training when provided with more computational resources.
- During the annealing phase, we use diverse and high-quality knowledge and ability-oriented SFT data, mixed into the pre-training data.

To validate the advantages of our training strategy, we conduct comparison experiments using (A) MiniCPM-2.4B’s intermediate checkpoint in the stable stage; and (B) MiniCPM-1.2B’s last checkpoints in the stable stage. Specifically, we compare the following:

1. A-1: 2.4B model, decay using only pre-training data, followed by 4B token SFT.
2. A-2: 2.4B model, decay using the aforementioned high-quality data unlabeled data and SFT data mixed into pre-training data, also followed by 4B token SFT.
3. B-1: 1.2B model, decay using only pre-training data, followed by 6B token SFT.
4. B-2: 1.2B model, decay using only pre-training data, followed by 12B token SFT.

-
5. B-3: 1.2B model, annealing using the aforementioned high-quality data + SFT data mixed into pre-training data, also followed by 6B token SFT.

The results of the experiments are shown in Table 2. We can see that, despite the A-2 and A-1 have undergone the same SFT distribution, adding SFT data to the decay stage pushes the boundary. Comparison between B-2 and B-3 demonstrate that the deficiency of only SFT is not due to the insufficient training tokens in SFT stage.

	C-Eval	CMMLU	MMLU	GSM8K	MATH	HumanEval	MBPP
A-1	40.0	41.5	44.6	27.7	5.1	27.7	24.4
A-2	52.6	51.1	50.9	42.3	5.4	30.4	30.3
B-1	40.9	41.5	47.9	34.2	7.9	43.9	30.5
B-2	41.2	42.0	47.9	34.4	7.3	43.9	29.8
B-3	49.1	46.8	49.6	31.8	10.5	44.5	32.8

Table 2: The ablation study of different training strategies.

The results indicate that the benefits of introducing high-quality data at the beginning of the decay stage are much higher than simply adding it during the SFT phase.

6 Model

6.1 Model Details

Vocabulary. We use two tokenizers of 122,753 vocabulary size for MiniCPM-2.4B and 73,440 vocabulary for MiniCPM-1.2B.

Shared Input-output Layer. For SLM, the embedding takes up a large parameter space. To make the model parameters smaller, we use the Embedding Sharing techniques for both MiniCPM-2.4B and MiniCPM-1.2B.

Deep-and-thin Network. We train MiniCPM-2.4B before training MiniCPM-1.2B. When training MiniCPM-2.4B, we adopt a deeper and thinner architecture compared to Phi-2 (Javaheripi & Bubeck, 2023) (40 layers compared to 32 layers). Recently, Liu et al. (2024) propose to train deep and thin networks for SLMs, which aligns with our perspective. Therefore, we further make the architecture deeper and thinner for MiniCPM-1.2B.

Group Query Attention. We train MiniCPM-2.4B without modification on the attention layer. Whereas we apply Group Query Attention (Ainslie et al., 2023) to MiniCPM-1.2B, inspired by Liu et al. (2024), to further reduce the parameters number.

Model	N (B)	d_m	d_{ff}	d_h	n_q	n_{kv}	L	Batch size (M)	Tokens (T)
MiniCPM-1.2B	1,247,442,432	1,536	3,840	64	24	8	52	2M → 4M	1.1T
MiniCPM-2.4B	2,442,057,984	2,304	5,760	64	36	36	40	4M	1.1T

Table 3: Model configurations for MiniCPM. N (B), d_m , d_{ff} , d_h , n_q , n_{kv} , L, Batch size (M), Tokens (T) represents the number of non-embedding parameters of the model, model hidden dimension, feedforward layer bottleneck dimension, attention head dimension, number of queries, number key/values, number of layers, training batch size, total training tokens.

6.2 Training Stages

Stable Training Stage. We utilize around 1T data (see Figure 12 for data distribution), with the majority of the data sourced from open datasets. We use the optimal configuration discovered during the model wind tunnel experiments, WSD LRS, with a batch size of 3.93 million and a max learning rate of 0.01.

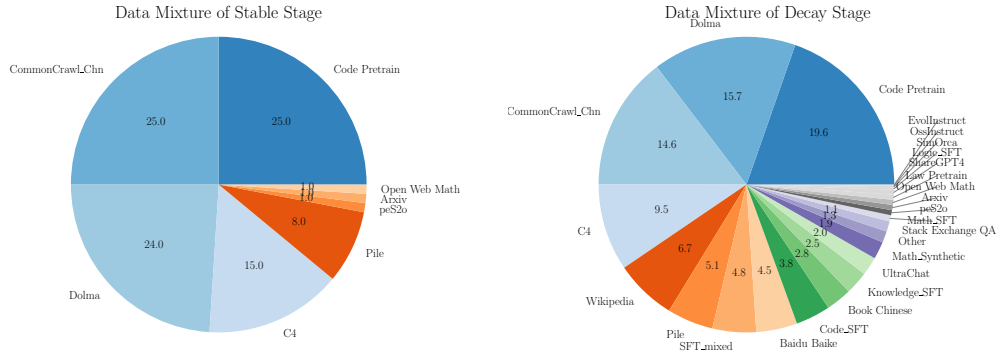


Figure 12: Data mixture of different training stages. The stable stage is shown on the left and the decay stage is shown on the right.

Decay Stage. We use a mixture of the pretraining data and high-quality SFT data. For the specific annealing form of the WSD scheduler, we employ exponential annealing, i.e. $f(s - T) = 0.5^{(s-S)/T}$, in which T is set to be 5000 steps (20B tokens).

SFT Stage. We find it still necessary to conduct a separate SFT phase. We utilize SFT data similar to the annealing phase excluding pre-training data and train with approximately 6 billion tokens. The learning rate for SFT is aligned with the one at the end of annealing, and a WSD Scheduler with exponential decay is also employed.

6.3 Training Data Distribution

We introduce our training data distribution in Figure 12. In the figure, CommonCrawl Chn in a Chinese Corpus is derived from CommonCrawl raw corpus and goes through thorough cleaning. Dolma (Soldaini et al., 2024), C4 (Raffel et al., 2019), and Pile (Gao et al., 2020; Biderman et al., 2022) are English corpora. They are deduplicated inner corpus and across corpus using MinHash algorithms (Broder, 1997). The Code Pre-train data contains the stack (Kocetkov et al., 2022) and StarCoder Li et al. (2023a), with inner deduplication and cross deduplication. In the decay stage, the data mixture contains more diverse data and proprietary data, including UltraChat (Ding et al., 2023), SlimOrca (Lian et al., 2023a;b), OssInstruct (Wei et al., 2023), EvoInstruct (Xu et al., 2023). The data with the suffix SFT is our proprietary data including LeetCode questions, Kindergarten through 12th grade (K12) textbooks and questions, etc.

6.4 Training Loss

The overall training loss on the C4 dataset is shown in Figure 13. We can see that as expected in the preliminary experiments, the loss decreases sharply in the decay stage. Since we use the exponential decay, the loss still drops after the learning rate drops below 10% of the max learning rate. However, since we continue to SFT the model after the decay stage, we do not utilize the final checkpoints. The checkpoints we finetune from are shown in the last checkpoint of dark green segment. The first drop in MiniCPM-1.2B is the result of enlarging batch size, which might have a similar effect as decreasing learning rate (Smith et al., 2017).

6.5 Evaluation

The overall evaluation utilizes our open-source tool UltraEval³. UltraEval is an open-source framework for assessing the capabilities of foundation models. The underlying inference and acceleration use the open-source framework vLLM (Kwon et al., 2023), and

³<https://ultraeval.openbmb.cn/home>

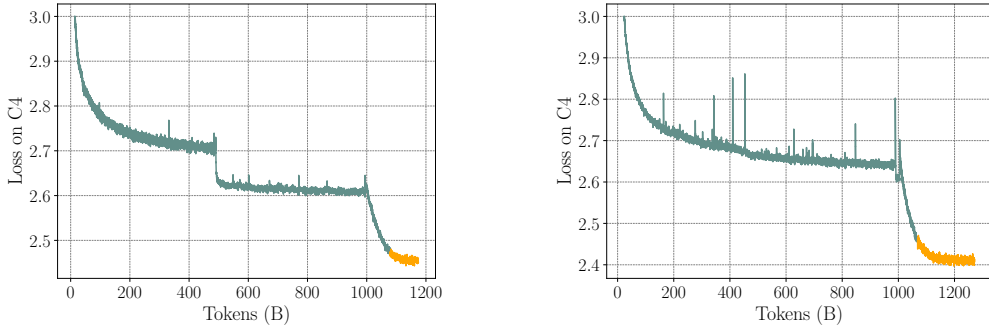


Figure 13: Loss curve on C4 dataset for MiniCPM-1.2B (Left) and MiniCPM-2.4B (Right). The orange segment at the tail of the loss curve represents the remaining decay process, which is not utilized in the released version of MiniCPM.

the dataset includes commonly used datasets: MMLU (Hendrycks et al., 2020) for English knowledge, CMMLU (Li et al., 2024) and C-Eval (Huang et al., 2024) for Chinese knowledge, HumanEval (Chen et al., 2021) and MBPP (Austin et al., 2021) for coding, GSM8K (Cobbe et al., 2021) and MATH (Hendrycks et al., 2021) for mathematics, and HellaSwag (Zellers et al., 2019), ARC-e (Clark et al., 2018), ARC-c (Clark et al., 2018) for commonsense reasoning, and BBH (Suzgun et al., 2022) for logic reasoning.

When testing QA tasks (ARC-e, ARC-c, HellaSwag), two approaches are typically employed. The first involves using Perplexity (PPL): we extend each option as the continuation of the question and use the PPL of the option as the selection criterion. The second is direct generation, where the model directly outputs answer options. We observe significant differences in results obtained using these two methods. To address this phenomenon, when reporting the scores for each model, we adopt the score from the evaluation method that yields the highest score, ensuring fairness in comparison.

The overall evaluation results are in Table 4. Generally, BBH is harder for SLMs than LLMs compared to another knowledge-oriented dataset, demonstrating that reasoning ability might be more dependent on model size than knowledge.

7 MiniCPM Family

7.1 MiniCPM-DPO

After SFT, we employ DPO (Rafailov et al., 2024) for human preference alignment of the model. During this stage, UltraFeedback (Cui et al., 2023) is utilized as the primary alignment dataset, and a proprietary preference dataset is constructed to enhance the model’s code and mathematical capabilities. We conduct one epoch of DPO training with a learning rate of 1×10^{-5} and utilize a Cosine LRS since we have a pre-defined training step.

7.2 MiniCPM-128K

Initialization. For the initialization, we disable sharing embeddings between input and output, primarily to accommodate vocabulary parallelism essential for training with long context. The LM head is initialized from the input embedding.

Training. Similar to MiniCPM, MiniCPM-2.4B-128K utilizes the WSD as its learning rate scheduler and reuses the last checkpoint of the stable training stage of MiniCPM-2.4B. Concerning training data, we categorize the dataset distribution detailed in Section 6.3 into “short data” and “long data”. We classify books, wikis, and papers as “long data”, and the other as the “short data”. The training comprises 44% long data and 56% short data for continued training. For the extension of long contexts, we apply Adjusted Base Frequency (ABF) (Xiong et al., 2023) in the 4K to 32k range and employ NTK-Aware RoPE Scaling (bloc97, 2023) and curriculum learning from 32K to 128K. Both two stages

Model	C-Eval	CMMLU	MMLU	HumanEval	MBPP	GSM8K	MATH
Llama2-7B	32.42	31.11	44.32	12.20	27.17	13.57	1.80
Qwen-7B	58.96	60.35	57.65	17.07	42.15	41.24	5.34
Deepseek-7B	42.82	44.45	47.82	20.12	41.45	15.85	1.53
Mistral-7B	46.12	42.96	62.69	27.44	45.20	33.13	5.00
Gemma-7B	42.57	44.20	60.83	38.41	50.12	47.31	6.18
Llama2-13B	37.32	37.06	54.71	17.07	32.55	21.15	2.25
MPT-30B	29.34	32.09	46.56	21.95	35.36	10.31	1.56
Falcon-40B	40.29	41.57	53.53	24.39	36.53	22.44	1.92
TinyLlama-1.1B	25.02	24.03	24.3	6.71	19.91	2.27	0.74
Qwen-1.8B	49.81	45.32	43.37	7.93	17.8	19.26	2.42
Qwen1.5-1.8B	55.00	50.85	43.81	5.49	24.82	26.16	3.25
Gemini Nano-3B	-	-	-	-	27.20	22.80	-
StableLM-Zephyr-3B	30.34	30.89	45.90	35.37	31.85	52.54	12.12
Phi-2(2B)	23.37	24.18	52.66	47.56	55.04	57.16	3.50
Gemma-2B	29.26	28.56	38.49	24.39	29.74	16.83	3.34
MiniCPM-1.2B	49.14	46.81	49.63	44.51	32.75	31.77	10.60
MiniCPM-2.4B	51.13	51.07	53.46	50.00	47.31	53.83	10.24
Model	BBH	ARC-e	ARC-c	HellaSwag	Avg	Avg _{gen}	Avg _{chn}
Llama2-7B	33.23	75.25 [†]	42.75	75.62 [†]	35.40	36.21	31.77
Qwen-7B	37.75	83.42	64.76	75.32 [†]	49.46	47.19	59.66
Deepseek-7B	33.38	74.58 [†]	42.15 [†]	75.45 [†]	39.96	39.15	43.64
Mistral-7B	41.06	83.92	70.73	80.43 [†]	48.97	49.96	44.54
Gemma-7B	39.19	89.35	76.79	79.47	52.22	54.18	43.39
Llama2-13B	37.92	78.87 [†]	58.19	79.23 [†]	41.48	42.44	37.19
MPT-30B	38.22	78.66 [†]	46.08 [†]	79.72 [†]	38.17	39.82	30.72
Falcon-40B	36.24	81.94 [†]	57.68	83.26 [†]	43.62	44.21	40.93
TinyLlama-1.1B	28.78	60.77 [†]	28.15 [†]	58.33 [†]	25.36	25.55	24.53
Qwen-1.8B	29.07	63.97 [†]	43.69	59.28 [†]	34.72	31.87	47.57
Qwen1.5-1.8B	28.82	64.86	45.56	59.39	37.09	33.57	52.93
Gemini Nano-3B	42.40	-	-	-	-	-	-
StableLM-Zephyr-3B	37.68	73.78	55.38	71.87 [†]	43.46	46.32	30.62
Phi-2(2B)	43.39	86.11	71.25	73.07[†]	48.84	54.42	23.78
Gemma-2B	30.93	74.33	40.70	69.51	35.10	36.47	28.91
MiniCPM-1.2B	34.70	80.93	66.81	54.72	45.67	45.16	47.98
MiniCPM-2.4B	36.87	85.44	68.00	68.25	52.33	52.60	51.10

Table 4: Benchmark Score of MiniCPM-2.4B and MiniCPM-1.2B (both without RLHF). The two tables are continuous horizontally. **Avg** is over all dataset in the table, **Avg_{chn}** is the average of C-Eval and CMMLU while **Avg_{gen}** is the average of remaining datasets. [†] means the result is tested using PPL metrics. **Bold** numbers represent the best score among the SLMs. Results of Gemini Nano-3B are borrowed from [Gemini et al. \(2023\)](#).

Model	C-Eval	CMMLU	MMLU	HumanEval	MBPP	GSM8K	MATH
ChatGLM2-6B	52.05	49.21	45.77	10.37	9.38	22.74	5.96
Mistral-7B-Instruct-v0.1	38.06	36.96	53.56	29.27	39.34	28.73	3.48
Mistral-7B-Instruct-v0.2	42.55	41.92	60.51	36.59	48.95	40.49	4.95
Qwen-7B-Chat	58.57	57.23	56.03	15.85	40.52	42.23	8.3
Yi-6B-Chat	70.88	71.11	62.95	14.02	28.34	36.54	3.88
Baichuan2-7B-Chat	53.28	53.50	53.00	21.34	32.32	25.25	6.32
Deepseek-7B-chat	46.95	49.72	51.67	40.85	48.48	48.52	4.26
Llama2-7B-Chat	34.54	32.64	47.64	14.02	27.40	21.15	2.08
MiniCPM-2.4B-DPO	48.64	48.37	53.05	51.22	48.01	53.37	9.86
Model	BBH	ARC-e	ARC-c	HellaSwag	Avg	Avg _{gen}	Avg _{chn}
ChatGLM2-6B	32.60	74.45	56.82	58.48 [†]	37.98	35.17	50.63
Mistral-7B-Instruct-v0.1	39.52	81.61	63.99	73.47 [†]	44.36	45.89	37.51
Mistral-7B-Instruct-v0.2	39.81	86.28	73.38	84.55 [†]	50.91	52.83	42.24
Qwen-7B-Chat	37.34	64.44 [†]	39.25 [†]	74.52 [†]	44.93	42.05	57.90
Yi-6B-Chat	37.43	84.89	70.39	74.60 [†]	50.46	45.89	71.00
Baichuan2-7B-Chat	37.46	79.63	60.15	69.23 [†]	44.68	42.74	53.39
Deepseek-7B-chat	35.70	76.85	63.05	76.68 [†]	49.34	49.56	48.34
Llama2-7B-Chat	35.54	74.28	54.78	75.65 [†]	38.16	39.17	33.59
MiniCPM-2.4B-DPO	36.22	85.02	68.17	65.67	51.60	52.29	48.51

Table 5: Benchmark scores for MiniCPM-2.4B-DPO compared with larger chat models.

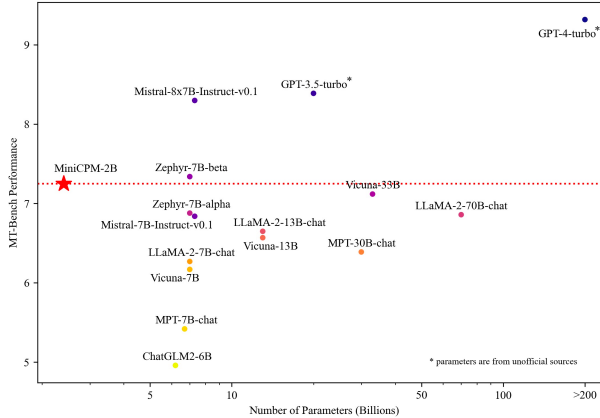


Figure 14: MTBench score of MiniCPM-DPO-2.4B surpasses many models of larger size.

involve future training. Furthermore, as indicated in Yi Tech Report (Young et al., 2024) and Zebra (Song et al., 2023), we use synthetic long QA data that significantly enhances model performance in context-aware tasks.

Evaluation. We evaluate MiniCPM-2.4B-128K in ∞ Bench (Zhang et al., 2024b), a pioneering benchmark for long context evaluations. **The tasks in ∞ Bench (Zhang et al., 2024b) extend beyond typical retrieval tasks and challenge the model with long context reasoning.** We can see in Table 6, we achieve comparable results in Mistral-7B-Instruct-v0.2 (ABF1000w) and outperform ChatGLM3-6B-128K despite being 2.5 times smaller.

Model	Passkey	Number String	KV Retrieval	Long Book Choice Eng	Long Book QA Chn	Long Book QA Eng	Long Book Sum Eng
LWM-Text-128K	100	97.8	0.6	28.82	15.93	14.31	9.99
Yarn-Mistral-7b-128K	92.71	56.61	0	27.95	15.49	9.55	9.06
Mistral-7B-Instruct-v0.2(ABF 1000w)	100	78.98	3.6	37.12	11.74	17.37	21.12
Yi-6B-200K	100	94.92	0	36.68	15.07	9.2	0.92
ChatGLM3-6B-128K	89.93	99.66	5.2	46.29	10.7	8.38	25.91
MiniCPM-2.4B-128K	98.31	99.83	9	29.69	23.06	16.33	15.73

Model	Long Dialogue QA Eng	Math Calc	Math Find	Code Debug	Code Run	Avg	Avg w/o Code & Math
LWM-Text-128k	1.5	0	3.43	20.05	1	24.45	33.62
Yarn-Mistral-7b-128k	7.5	0	17.14	0.76	1.25	19.84	27.36
Mistral-7B-Instruct-v0.2(ABF 1000w)	9.5	0	29.43	17.51	0	27.75	36.9
Yi-6B-200K	3.5	0	4.29	0.51	0.75	22.15	32.54
ChatGLM3-6B-128K	6.5	0	8	5.33	1	25.58	36.57
MiniCPM-2.4B-128K	9.5	0	4.29	22.08	0	27.32	37.68

Table 6: MiniCPM-2.4B-128K result in ∞ Bench (Zhang et al., 2024b)

7.3 MiniCPM-MoE

Initialization. MiniCPM-MoE is initialized utilizing Sparse Upcycling (Komatsuzaki et al., 2022). The dense model checkpoint, derived from the stable phase of MiniCPM, undergoes a transformation wherein each MLP layer is substituted by an MoE layer. These new MoE layers are exact replicas of the original MLP layers from the dense checkpoint. The router parameters are randomly initialized following a normal distribution with a mean of 0 and a variance of 0.01.

Routing Mechanism. The number of total non-embedding parameters of MiniCPM-MoE is 13.6B. During training and inference, two out of eight experts are activated for each token, resulting in the number of activated parameters being approximately 4B. To prevent training from collapsing, an additional load balancing loss (Fedus et al., 2022) is applied to the final training objective. This auxiliary loss is multiplied by 0.01 which is large enough to ensure a balanced distribution of tokens assigned to different experts.

Training. Similar to MiniCPM, we employ WSD as our learning rate scheduler. Regarding the training data, we adhere strictly to the distribution specified in Section 6.3. The training batch size is maintained at 4M tokens during the stable training and decay stages and is reduced to 2M tokens during the SFT stage. The pre-training phase (including continue pre-train and decay stage) spans 130K steps, after which we notice diminishing improvement. The benchmark results are detailed in Table 7.

Model	C-Eval	CMMLU	MMLU	HumanEval	MBPP	GSM8K	MATH	BBH
Llama2-34B	-	-	62.6	22.6	33.0 [†]	42.2	6.24	44.1
Deepseek-MoE (16B)	40.6	42.5	45.0	26.8	39.2	18.8	4.3	-
Mistral-7B	46.12	42.96	62.69	27.44	45.20	33.13	5.0	41.06
Gemma-7B	42.57	44.20	60.83	38.41	50.12	47.31	6.18	39.19
MiniCPM-2.4B	51.13	51.07	53.46	50.00	47.31	53.83	10.24	36.87
MiniCPM-MoE (13.6B)	58.11	58.80	58.90	56.71	51.05	61.56	10.52	39.22

Table 7: Benchmark results of MiniCPM-MoE. [†] means evaluation results on the full set of MBPP, instead of the hand-verified set (Austin et al., 2021). The evaluation results of Llama2-34B and Qwen1.5-7B are taken from their technical reports.

References

Josh Achiam, Steven Adler, Sandhini Agarwal, Lama Ahmad, Ilge Akkaya, Florencia Leoni Aleman, Diogo Almeida, Janko Altenschmidt, Sam Altman, Shyamal Anadkat, et al. Gpt-4 technical report. [arXiv preprint arXiv:2303.08774](#), 2023.

Armen Aghajanyan, Lili Yu, Alexis Conneau, Wei-Ning Hsu, Karen Hambardzumyan, Susan Zhang, Stephen Roller, Naman Goyal, Omer Levy, and Luke Zettlemoyer. Scaling laws for generative mixed-modal language models. In [International Conference on Machine Learning](#), pp. 265–279. PMLR, 2023.

Joshua Ainslie, James Lee-Thorp, Michiel de Jong, Yury Zemlyanskiy, Federico Lebron, and Sumit Sanghai. GQA: Training generalized multi-query transformer models from multi-head checkpoints. In Houda Bouamor, Juan Pino, and Kalika Bali (eds.), [Proceedings of the 2023 Conference on Empirical Methods in Natural Language Processing](#), pp. 4895–4901, Singapore, December 2023. Association for Computational Linguistics. doi: 10.18653/v1/2023.emnlp-main.298. URL <https://aclanthology.org/2023.emnlp-main.298>.

Ebtessam Almazrouei, Hamza Alobeidli, Abdulaziz Alshamsi, Alessandro Cappelli, Ruxandra Cojocaru, Mérourane Debbah, Étienne Goffinet, Daniel Hesslow, Julien Launay, Quentin Malartic, et al. The falcon series of open language models. [arXiv preprint arXiv:2311.16867](#), 2023.

Jacob Austin, Augustus Odena, Maxwell Nye, Maarten Bosma, Henryk Michalewski, David Dohan, Ellen Jiang, Carrie Cai, Michael Terry, Quoc Le, and Charles Sutton. Program synthesis with large language models, 2021.

Jinze Bai, Shuai Bai, Yunfei Chu, Zeyu Cui, Kai Dang, Xiaodong Deng, Yang Fan, Wenbin Ge, Yu Han, Fei Huang, et al. Qwen technical report. [arXiv preprint arXiv:2309.16609](#), 2023.

Jeanine Banks and Tris Warkentin. Gemma: Introducing new state-of-the-art open models. <https://blog.google/technology/developers/gemma-open-models/>, 2024. Accessed: date-of-access.

Xiao Bi, Deli Chen, Guanting Chen, Shanhuang Chen, Damai Dai, Chengqi Deng, Honghui Ding, Kai Dong, Qiushi Du, Zhe Fu, et al. Deepseek llm: Scaling open-source language models with longtermism. [arXiv preprint arXiv:2401.02954](#), 2024.

Stella Biderman, Kieran Bicheno, and Leo Gao. Datasheet for the pile. [arXiv preprint arXiv:2201.07311](#), 2022.

bloc97. NTK-Aware Scaled RoPE allows LLaMA models to have extended (8k+) context size without any fine-tuning and minimal perplexity degradation. https://www.reddit.com/r/LocalLLaMA/comments/141z7j5/ntkaware_scaled_rope_allows_llama_models_to_have/, 2023. Accessed: [Insert Date of Access].

Andrei Z Broder. On the resemblance and containment of documents. In *Proceedings. Compression and Complexity of SEQUENCES 1997* (Cat. No. 97TB100171), pp. 21–29. IEEE, 1997.

Mark Chen, Jerry Tworek, Heewoo Jun, Qiming Yuan, Henrique Ponde de Oliveira Pinto, Jared Kaplan, Harri Edwards, Yuri Burda, Nicholas Joseph, Greg Brockman, et al. Evaluating large language models trained on code. [arXiv preprint arXiv:2107.03374](#), 2021.

Peter Clark, Isaac Cowhey, Oren Etzioni, Tushar Khot, Ashish Sabharwal, Carissa Schoenick, and Oyvind Tafjord. Think you have solved question answering? try arc, the ai2 reasoning challenge. [arXiv preprint arXiv:1803.05457](#), 2018.

Karl Cobbe, Vineet Kosaraju, Mohammad Bavarian, Mark Chen, Heewoo Jun, Lukasz Kaiser, Matthias Plappert, Jerry Tworek, Jacob Hilton, Reiichiro Nakano, et al. Training verifiers to solve math word problems. [arXiv preprint arXiv:2110.14168](#), 2021.

Ganqu Cui, Lifan Yuan, Ning Ding, Guanming Yao, Wei Zhu, Yuan Ni, Guotong Xie, Zhiyuan Liu, and Maosong Sun. Ultrafeedback: Boosting language models with high-quality feedback, 2023.

Nolan Dey, Gurnpreet Gosal, Hemant Khachane, William Marshall, Ribhu Pathria, Marvin Tom, Joel Hestness, et al. Cerebras-gpt: Open compute-optimal language models trained on the cerebras wafer-scale cluster. [arXiv preprint arXiv:2304.03208](#), 2023.

Ning Ding, Yulin Chen, Bokai Xu, Yujia Qin, Zhi Zheng, Shengding Hu, Zhiyuan Liu, Maosong Sun, and Bowen Zhou. Enhancing chat language models by scaling high-quality instructional conversations, 2023.

Zhengxiao Du, Aohan Zeng, Yuxiao Dong, and Jie Tang. Understanding emergent abilities of language models from the loss perspective. [arXiv preprint arXiv:2403.15796](#), 2024.

William Fedus, Barret Zoph, and Noam Shazeer. Switch transformers: Scaling to trillion parameter models with simple and efficient sparsity. *Journal of Machine Learning Research*, 23(120):1–39, 2022.

Elias Frantar, Saleh Ashkboos, Torsten Hoefer, and Dan Alistarh. GPTQ: accurate post-training quantization for generative pre-trained transformers. *CoRR*, abs/2210.17323, 2022. doi: 10.48550/ARXIV.2210.17323. URL <https://doi.org/10.48550/arXiv.2210.17323>.

Leo Gao, Stella Biderman, Sid Black, Laurence Golding, Travis Hoppe, Charles Foster, Jason Phang, Horace He, Anish Thite, Noa Nabeshima, et al. The Pile: An 800GB dataset of diverse text for language modeling. [arXiv preprint arXiv:2101.00027](#), 2020.

Team Gemini, Rohan Anil, Sebastian Borgeaud, Yonghui Wu, Jean-Baptiste Alayrac, Jiahui Yu, Radu Soricut, Johan Schalkwyk, Andrew M Dai, Anja Hauth, et al. Gemini: a family of highly capable multimodal models. [arXiv preprint arXiv:2312.11805](#), 2023.

Suriya Gunasekar, Yi Zhang, Jyoti Aneja, Caio César Teodoro Mendes, Allie Del Giorno, Sivakanth Gopi, Mojan Javaheripi, Piero Kauffmann, Gustavo de Rosa, Olli Saarikivi, et al. Textbooks are all you need. [arXiv preprint arXiv:2306.11644](#), 2023.

Dan Hendrycks, Collin Burns, Steven Basart, Andy Zou, Mantas Mazeika, Dawn Song, and Jacob Steinhardt. Measuring massive multitask language understanding. [arXiv preprint arXiv:2009.03300](#), 2020.

Dan Hendrycks, Collin Burns, Saurav Kadavath, Akul Arora, Steven Basart, Eric Tang, Dawn Song, and Jacob Steinhardt. Measuring mathematical problem solving with the math dataset. [arXiv preprint arXiv:2103.03874](#), 2021.

Alex Henry, Prudhvi Raj Dachapally, Shubham Shantaram Pawar, and Yuxuan Chen. Query-key normalization for transformers. In Trevor Cohn, Yulan He, and Yang Liu (eds.), *Findings of the Association for Computational Linguistics: EMNLP 2020*, pp. 4246–4253, Online, November 2020. Association for Computational Linguistics. doi: 10.18653/v1/2020.findings-emnlp.379. URL <https://aclanthology.org/2020.findings-emnlp.379>.

Jordan Hoffmann, Sebastian Borgeaud, Arthur Mensch, Elena Buchatskaya, Trevor Cai, Eliza Rutherford, Diego de Las Casas, Lisa Anne Hendricks, Johannes Welbl, Aidan Clark, et al. Training compute-optimal large language models. *arXiv preprint arXiv:2203.15556*, 2022.

Jeremy Howard and Sebastian Ruder. Universal language model fine-tuning for text classification. *arXiv preprint arXiv:1801.06146*, 2018.

Shengding Hu, Xin Liu, Xu Han, Xirong Zhang, Chaoqun He, Weilin Zhao, Yankai Lin, Ning Ding, Zebin Ou, Guoyang Zeng, et al. Unlock predictable scaling from emergent abilities. *arXiv preprint arXiv:2310.03262*, 2023.

Yuzhen Huang, Yuzhuo Bai, Zhihao Zhu, Junlei Zhang, Jinghan Zhang, Tangjun Su, Junteng Liu, Chuancheng Lv, Yikai Zhang, Yao Fu, et al. C-eval: A multi-level multi-discipline chinese evaluation suite for foundation models. *Advances in Neural Information Processing Systems*, 36, 2024.

Andrew Hundt, Varun Jain, and Gregory D Hager. sharpdarts: Faster and more accurate differentiable architecture search. *arXiv preprint arXiv:1903.09900*, 2019.

Mojan Javaheripi and Sébastien Bubeck. Phi-2: The surprising power of small language models. <https://www.microsoft.com/en-us/research/blog/phi-2-the-surprising-power-of-small-language-models/>, 2023. Accessed: date-of-access.

Albert Q Jiang, Alexandre Sablayrolles, Arthur Mensch, Chris Bamford, Devendra Singh Chaplot, Diego de las Casas, Florian Bressand, Gianna Lengyel, Guillaume Lample, Lucile Saulnier, et al. Mistral 7b. *arXiv preprint arXiv:2310.06825*, 2023.

Jared Kaplan, Sam McCandlish, Tom Henighan, Tom B Brown, Benjamin Chess, Rewon Child, Scott Gray, Alec Radford, Jeffrey Wu, and Dario Amodei. Scaling laws for neural language models. *arXiv preprint arXiv:2001.08361*, 2020.

Denis Kocetkov, Raymond Li, Loubna Ben Allal, Jia Li, Chenghao Mou, Carlos Muñoz Ferrandis, Yacine Jernite, Margaret Mitchell, Sean Hughes, Thomas Wolf, Dzmitry Bahdanau, Leandro von Werra, and Harm de Vries. The stack: 3 tb of permissively licensed source code. Preprint, 2022.

Aran Komatsuzaki, Joan Puigcerver, James Lee-Thorp, Carlos Riquelme Ruiz, Basil Mustafa, Joshua Ainslie, Yi Tay, Mostafa Dehghani, and Neil Houlsby. Sparse upcycling: Training mixture-of-experts from dense checkpoints. *arXiv preprint arXiv:2212.05055*, 2022.

Woosuk Kwon, Zhuohan Li, Siyuan Zhuang, Ying Sheng, Lianmin Zheng, Cody Hao Yu, Joseph Gonzalez, Hao Zhang, and Ion Stoica. Efficient memory management for large language model serving with pagedattention. In *Proceedings of the 29th Symposium on Operating Systems Principles*, pp. 611–626, 2023.

Haonan Li, Yixuan Zhang, Fajri Koto, Yifei Yang, Hai Zhao, Yeyun Gong, Nan Duan, and Timothy Baldwin. Cmmlu: Measuring massive multitask language understanding in chinese, 2024.

Raymond Li, Loubna Ben Allal, Yangtian Zi, Niklas Muennighoff, Denis Kocetkov, Chenghao Mou, Marc Marone, Christopher Akiki, Jia Li, Jenny Chim, et al. Starcoder: may the source be with you! *arXiv preprint arXiv:2305.06161*, 2023a.

-
- Yuanzhi Li, Sébastien Bubeck, Ronen Eldan, Allie Del Giorno, Suriya Gunasekar, and Yin Tat Lee. Textbooks are all you need ii: phi-1.5 technical report. [arXiv preprint arXiv:2309.05463](https://arxiv.org/abs/2309.05463), 2023b.
- Wing Lian, Guan Wang, Bleys Goodson, Eugene Pentland, Austin Cook, Chanvichet Vong, and "Teknium". Slimorca: An open dataset of gpt-4 augmented flan reasoning traces, with verification, 2023a. URL <https://huggingface.co/Open-Orca/SlimOrca>.
- Wing Lian, Guan Wang, Bleys Goodson, Eugene Pentland, Austin Cook, Chanvichet Vong, "Teknium", and Nathan Hoos. Slimorca dedup: A deduplicated subset of slimorca, 2023b. URL <https://huggingface.co/datasets/Open-Orca/SlimOrca-Dedup/>.
- Zechun Liu, Changsheng Zhao, Forrest Iandola, Chen Lai, Yuandong Tian, Igor Fedorov, Yunyang Xiong, Ernie Chang, Yangyang Shi, Raghuraman Krishnamoorthi, et al. Mobilellm: Optimizing sub-billion parameter language models for on-device use cases. [arXiv preprint arXiv:2402.14905](https://arxiv.org/abs/2402.14905), 2024.
- Ilya Loshchilov and Frank Hutter. Sgdr: Stochastic gradient descent with warm restarts. [arXiv preprint arXiv:1608.03983](https://arxiv.org/abs/1608.03983), 2016.
- Ilya Loshchilov and Frank Hutter. Decoupled weight decay regularization. [arXiv preprint arXiv:1711.05101](https://arxiv.org/abs/1711.05101), 2017.
- Jack W Rae, Sebastian Borgeaud, Trevor Cai, Katie Millican, Jordan Hoffmann, Francis Song, John Aslanides, Sarah Henderson, Roman Ring, Susannah Young, et al. Scaling language models: Methods, analysis & insights from training gopher. [arXiv preprint arXiv:2112.11446](https://arxiv.org/abs/2112.11446), 2021.
- Rafael Rafailov, Archit Sharma, Eric Mitchell, Christopher D Manning, Stefano Ermon, and Chelsea Finn. Direct preference optimization: Your language model is secretly a reward model. [Advances in Neural Information Processing Systems](https://advancesinneuralinformationprocessingsystems.org/paper/2024/36), 36, 2024.
- Colin Raffel, Noam Shazeer, Adam Roberts, Katherine Lee, Sharan Narang, Michael Matena, Yanqi Zhou, Wei Li, and Peter J. Liu. Exploring the limits of transfer learning with a unified text-to-text transformer. [arXiv e-prints](https://arxiv.org/abs/1910.13462), 2019.
- Colin Raffel, Noam Shazeer, Adam Roberts, Katherine Lee, Sharan Narang, Michael Matena, Yanqi Zhou, Wei Li, and Peter J Liu. Exploring the limits of transfer learning with a unified text-to-text transformer. [Journal of machine learning research](https://jmlr.org/papers/v21/140.html), 21(140):1–67, 2020.
- Nikhil Sardana and Jonathan Frankle. Beyond chinchilla-optimal: Accounting for inference in language model scaling laws. [arXiv preprint arXiv:2401.00448](https://arxiv.org/abs/2401.00448), 2023.
- Rico Sennrich, Barry Haddow, and Alexandra Birch. Neural machine translation of rare words with subword units. In Katrin Erk and Noah A. Smith (eds.), [Proceedings of the 54th Annual Meeting of the Association for Computational Linguistics \(Volume 1: Long Papers\)](https://aclanthology.org/P16-1162), pp. 1715–1725, Berlin, Germany, August 2016. Association for Computational Linguistics. doi: 10.18653/v1/P16-1162. URL <https://aclanthology.org/P16-1162>.
- Weijia Shi, Sewon Min, Maria Lomeli, Chunting Zhou, Margaret Li, Victoria Lin, Noah A Smith, Luke Zettlemoyer, Scott Yih, and Mike Lewis. In-context pretraining: Language modeling beyond document boundaries. [arXiv preprint arXiv:2310.10638](https://arxiv.org/abs/2310.10638), 2023.
- Samuel L Smith, Pieter-Jan Kindermans, Chris Ying, and Quoc V Le. Don't decay the learning rate, increase the batch size. [arXiv preprint arXiv:1711.00489](https://arxiv.org/abs/1711.00489), 2017.
- Luca Soldaini, Rodney Kinney, Akshita Bhagia, Dustin Schwenk, David Atkinson, Russell Author, Ben Bogin, Khyathi Chandu, Jennifer Dumas, Yanai Elazar, Valentin Hofmann, Ananya Harsh Jha, Sachin Kumar, Li Lucy, Xinxi Lyu, Nathan Lambert, Ian Magnusson, Jacob Morrison, Niklas Muennighoff, Aakanksha Naik, Crystal Nam, Matthew E. Peters, Abhilasha Ravichander, Kyle Richardson, Zejiang Shen, Emma Strubell, Nishant Subramani, Oyvind Tafjord, Pete Walsh, Luke Zettlemoyer, Noah A. Smith, Hannaneh Hajishirzi, Iz Beltagy, Dirk Groeneveld, Jesse Dodge, and Kyle Lo. Dolma: An Open Corpus of Three Trillion Tokens for Language Model Pretraining Research. [arXiv preprint](https://arxiv.org/abs/2402.00159), 2024. URL <https://arxiv.org/abs/2402.00159>.

Kaiqiang Song, Xiaoyang Wang, Sangwoo Cho, Xiaoman Pan, and Dong Yu. Zebra: Extending context window with layerwise grouped local-global attention. [arXiv preprint arXiv:2312.08618](#), 2023.

Mirac Suzgun, Nathan Scales, Nathanael Schärli, Sebastian Gehrmann, Yi Tay, Hyung Won Chung, Aakanksha Chowdhery, Quoc V. Le, Ed H. Chi, Denny Zhou, and Jason Wei. Challenging big-bench tasks and whether chain-of-thought can solve them, 2022.

LLMFarm team. LLMFarm, 2023a. URL <https://github.com/guinmoon/LLMFarm>.

MLC team. MLC-LLM, 2023b. URL <https://github.com/mlc-ai/mlc-llm>.

Hugo Touvron, Thibaut Lavril, Gautier Izacard, Xavier Martinet, Marie-Anne Lachaux, Timothée Lacroix, Baptiste Rozière, Naman Goyal, Eric Hambro, Faisal Azhar, et al. Llama: Open and efficient foundation language models. [arXiv preprint arXiv:2302.13971](#), 2023.

Yuxiang Wei, Zhe Wang, Jiawei Liu, Yifeng Ding, and Lingming Zhang. Magicoder: Source code is all you need. [arXiv preprint arXiv:2312.02120](#), 2023.

Mitchell Wortsman, Peter J Liu, Lechao Xiao, Katie Everett, Alex Alemi, Ben Adlam, John D Co-Reyes, Izzeddin Gur, Abhishek Kumar, Roman Novak, et al. Small-scale proxies for large-scale transformer training instabilities. [arXiv preprint arXiv:2309.14322](#), 2023.

Mengzhou Xia, Tianyu Gao, Zhiyuan Zeng, and Danqi Chen. Sheared llama: Accelerating language model pre-training via structured pruning. [arXiv preprint arXiv:2310.06694](#), 2023.

Sang Michael Xie, Hieu Pham, Xuanyi Dong, Nan Du, Hanxiao Liu, Yifeng Lu, Percy S Liang, Quoc V Le, Tengyu Ma, and Adams Wei Yu. Doremi: Optimizing data mixtures speeds up language model pretraining. [Advances in Neural Information Processing Systems](#), 36, 2024.

Wenhan Xiong, Jingyu Liu, Igor Molybog, Hejia Zhang, Prajjwal Bhargava, Rui Hou, Louis Martin, Rashi Rungta, Karthik Abinav Sankararaman, Barlas Oguz, et al. Effective long-context scaling of foundation models. [arXiv preprint arXiv:2309.16039](#), 2023.

Can Xu, Qingfeng Sun, Kai Zheng, Xiubo Geng, Pu Zhao, Jiazhan Feng, Chongyang Tao, and Daxin Jiang. Wizardlm: Empowering large language models to follow complex instructions. [arXiv preprint arXiv:2304.12244](#), 2023.

Greg Yang, Edward J Hu, Igor Babuschkin, Szymon Sidor, Xiaodong Liu, David Farhi, Nick Ryder, Jakub Pachocki, Weizhu Chen, and Jianfeng Gao. Tensor programs v: Tuning large neural networks via zero-shot hyperparameter transfer. [arXiv preprint arXiv:2203.03466](#), 2022.

Greg Yang, Dingli Yu, Chen Zhu, and Soufiane Hayou. Tensor programs vi: Feature learning in infinite-depth neural networks. [arXiv preprint arXiv:2310.02244](#), 2023.

Jiasheng Ye, Peiju Liu, Tianxiang Sun, Yunhua Zhou, Jun Zhan, and Xipeng Qiu. Data mixing laws: Optimizing data mixtures by predicting language modeling performance. [arXiv preprint arXiv:2403.16952](#), 2024.

Alex Young, Bei Chen, Chao Li, Chengen Huang, Ge Zhang, Guanwei Zhang, Heng Li, Jiangcheng Zhu, Jianqun Chen, Jing Chang, et al. Yi: Open foundation models by 01. ai. [arXiv preprint arXiv:2403.04652](#), 2024.

Rowan Zellers, Ari Holtzman, Yonatan Bisk, Ali Farhadi, and Yejin Choi. Hellaswag: Can a machine really finish your sentence? [arXiv preprint arXiv:1905.07830](#), 2019.

Peiyuan Zhang, Guangtao Zeng, Tianduo Wang, and Wei Lu. Tinyllama: An open-source small language model. [arXiv preprint arXiv:2401.02385](#), 2024a.

Xinrong Zhang, Yingfa Chen, Shengding Hu, Zihang Xu, Junhao Chen, Moo Khai Hao, Xu Han, Zhen Leng Thai, Shuo Wang, Zhiyuan Liu, et al. ∞ bench: Extending long context evaluation beyond 100k tokens. [arXiv preprint arXiv:2402.13718](#), 2024b.

A Additional Results in Model Wind Tunnel Experiments

A.1 μ P hyper-parameter search

Meanwhile, we also try QK-Norm (Henry et al., 2020) and independent weight decay (Loshchilov & Hutter, 2017) as well to stabilize the learning rate. The overall results are shown in Figure 15. After applying the QK-norm, we observe a significant decrease in the learning rate sensitivity similar to Wortsman et al. (2023). In Figure 15, we identify the best hyper-parameters for $scale_depth = 1.4$, $scale_emb = 12$, $init_std = 0.1$, and $lr = 0.01$.

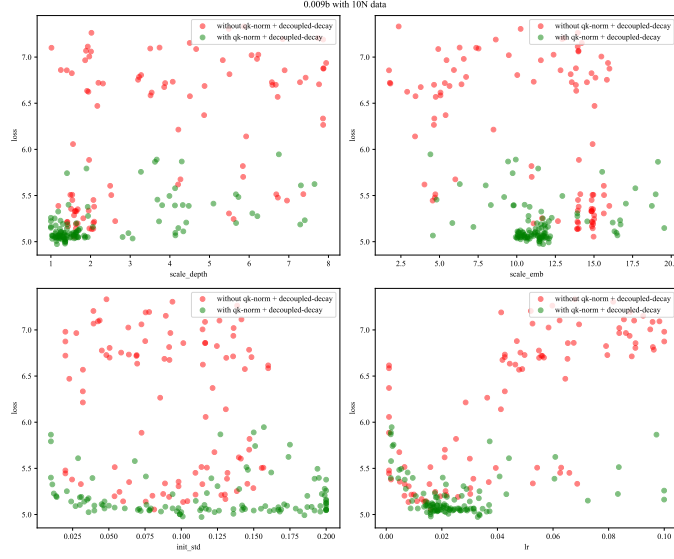


Figure 15: Grid search over the μ P parameterization spaces.

A.2 Model Architecture in Model Wind Tunnel Experiments

We list the model configuration used in the model wind tunnel experiments in Table 8.

Name	N (B)	d_m	d_{ff}	d_h	n_h	L
9M	0.009	320	800	64	5	8
30M	0.036	512	1280	64	8	12
70M	0.066	640	1600	64	10	14
0.1B	0.109	768	1920	64	12	16
0.17B	0.166	896	2240	64	14	18
0.2B	0.241	1024	2560	64	16	20
0.5B	0.499	1344	3360	64	21	24

Table 8: Model configurations and training configurations of the models in the scaling curve. N(B) represents the number of non-embedding parameters of the models, measured in billions.

B Additional Illustration on WSD LRS

B.1 Learning Rate Paradigm for Different LRSs

In this paper, we describe three kinds of LRSs, $\text{Cosine}(T)$, $\text{CosineLoop}(T)$, and $\text{WSD}(T, D)$. Cosine and Cosine Loop take the form of the following:

$$\begin{aligned} \text{Cosine}(T; s) = \\ \begin{cases} \frac{s}{W}\eta, & s < W \\ 0.9\eta\cos(\pi\frac{s}{T}) + 0.1\eta, & W < s < T \\ 0.1\eta, & s > T \end{cases} \end{aligned}$$

$$\begin{aligned} \text{CosineLoop}(T; s) = \\ \begin{cases} \frac{s}{W}\eta, & s < W \\ 0.9\eta\cos(\pi\frac{s}{T}) + 0.1\eta, & W < s \\ 0.1\eta, & s > T \end{cases} \end{aligned}$$

An illustrative learning rate diagram for WSD and Cosine Scheduler is shown in Figure 16.

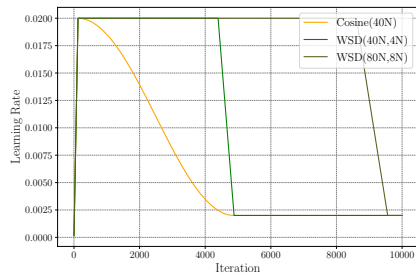


Figure 16: Illustrative comparison between Cosine LRS and WSD LRS. The WSD LRS with different end steps share the same stable training stage.

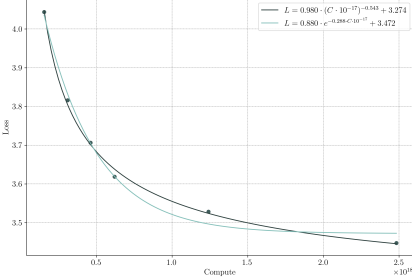


Figure 17: We use two different function forms to fit the data scaling law achieved by WSD LRS and choose power law as the best fit.

B.2 Fitting the Data Scaling Law

In this section, we describe the fitted data scaling law for continue training with WSD LRS. Each point in Figure 17 is the end of the decay stage in WSD LRS with a different end step. We try two function forms: exponential and polynomial. The fitted result shows that the polynomial scaling law is still the best for continue training.

C MiniCPM’s Vocabulary

For the 2.4B model, we use a tokenizer consisting of 122,753 tokens (denoted by MiniCPMTOKENIZER-120K). This vocabulary is constructed from extensive and diverse language data, utilizing the sentencepiece library ⁴ for Byte Pair Encoding (BPE) (Sennrich et al., 2016), and includes special symbols like traditional Chinese characters, rare characters, emojis, and special symbols such as Greek letters, Cyrillic letters, etc.

For our 1.2B model, we use a smaller vocab MiniCPMTOKENIZER-70K. Compared to the MiniCPMTOKENIZER-120K tokenizer, we have re-trained the tokenization on the same documents, while setting the max number of vocabs to 64,000. For the special characters, we only add the traditional Chinese characters, emojis, and special symbols, but leave out the rare characters in Chinese.

We conduct evaluations on 300,000 documents in Chinese, English, code, and academic papers that are not in the training set of the Tokenizer. The MiniCPM-120K tokenizer achieves the highest compression ratio (Bytes/Tokens).

D Quantization

We conduct 4-bit quantization on our model. We do not quantize the parameters of embedding and layer normalization, since the performance of the model is sensitive to these

⁴<https://github.com/google/sentencepiece>

	Baichuan2	ChatGLM2	Llama2	MiniCPM-120K	MiniCPM-70K
Vocab Size	125,696	64,794	32,000	122,753	73,440
Compression Rate (Bytes/Tokens)					
Chinese	3.64	3.54	1.87	3.73	3.56
English	4.12	4.02	3.78	4.14	4.02
Code	2.71	2.71	2.74	2.81	2.76
Paper	2.74	2.88	2.97	2.93	2.88
Average	3.30	3.29	2.84	3.40	3.31

Table 9: Compression ratio comparison.

parameters. Therefore, we only need to quantify each weight matrix. Denote the weight matrix as $\mathbf{W} \in \mathbb{R}^{d_{out} \times d_{in}}$. We group every G consecutive parameter at the d_{in} dimension and form d_{in}/G group. Then we quantize each group of the parameters separately. For each group parameter \mathbf{w} , we calculate the quantization scale and zero point as follows:

$$\text{scale} = \frac{\max(\mathbf{w}) - \min(\mathbf{w})}{2^4 - 1}, \text{zero} = -\frac{\min(\mathbf{w})}{\text{scale}} - 2^3.$$

Group parameter \mathbf{w} are then quantized to

$$\hat{w} = \text{quant}(w) = \text{round}\left(\frac{w}{\text{scale}} + \text{zero}\right),$$

where *round* operation round a floating point to nearest integer. The dequantization operation is approximately the reverse of the quantization method, which is

$$\text{dequant}(\hat{w}) = \text{scale}(\hat{w} - \text{zero}).$$

Finally, matrix $\mathbf{W} \in \mathbb{R}^{d_{out} \times d_{in}}$ is quantized to int4 $\hat{\mathbf{W}} \in \mathbb{R}^{d_{out} \times d_{in}}$, float $\text{scale} \in \mathbb{R}^{d_{out} \times \frac{d_{in}}{G}}$ and float $\text{zero} \in \mathbb{R}^{d_{out} \times \frac{d_{in}}{G}}$.

To reduce the quantization loss, we adopt GPTQ (Frantar et al., 2022) to apply weight calibration. We sample calibration data \mathbf{X} from a similar distribution of SFT data. The quantization objective is to minimize the disturbance of the quantization $\|\mathbf{WX} - \text{dequant}(\hat{\mathbf{W}})\mathbf{X}\|_2^2$. We follow GPTQ to quantize weight iteratively and update the remaining non-quantized weight by

$$\delta_F = -\frac{w_q - \text{dequant}(\text{quant}(w_q))}{[H_F^{-1}]_{qq}} \cdot (H_F^{-1})_{:,q},$$

where q is the quantization position in the current iteration while F denotes the remaining non-quantized weights. H_F is the hessian matrix of the objective function.

E Edge Device Benchmarking

After Int4 quantization in Appendix D, MiniCPM-2.4B’s footprint is reduced to 2GB, facilitating deployment on mobile edge devices. We adapted the model for Android and HarmonyOS using MLC-LLM (team, 2023b) and employed LLMFarm (team, 2023a) for adaptation to the iPhone system. This adaptation was tested on various edge mobile devices.

The result is shown in Table 10, we can see that on the most advanced smartphone iPhone 15 Pro, the inference throughput is as high as 18 tokens per second. In other devices, the inference throughput is also acceptable.

F Case Demonstration

SmartPhone	Operating System	Processor	Phone Memory (GB)	Inference Throughput (token/s)
OPPO Find N3	Android 13	snapdragon 8 Gen2	12	6.5
Samsung S23 Ultra	Android 14	snapdragon 8 Gen2	12	6.4
Meizu M182Q	Android 11	snapdragon 888Plus	8	3.7
Xiaomi 12 Pro	Android 13	snapdragon 8 Gen1	8+3	3.7
Xiaomi Redmi K40	Android 11	snapdragon 870	8	3.5
Oneplus LE 2100	Android 13	snapdragon 870	12	3.5
Oneplus HD1900	Android 11	snapdragon 865	8	3.2
Oneplus HD1900	Android 11	snapdragon 855	8	3.0
Oneplus HD1905	Android 10	snapdragon 855	8	3.0
Oneplus HD1900	Android 11	snapdragon 855	8	3.0
Xiaomi MI 8	Android 9	snapdragon 845	6	2.3
Huawei Nova 11SE	Harmony 4.0.0	snapdragon 778	12	1.9
Xiaomi MIX 2	Android 9	snapdragon 835	6	1.3
iPhone 15 Pro	iOS 17.2.1	A17 pro	8	18.0
iPhone 15	iOS 17.2.1	A16	6	15.0
iPhone 12 Pro	iOS 16.5.1	A14	6	5.8
iPhone 12	iOS 17.2.1	A14	4	5.8
iPhone 11	iOS 16.6	A13	4	4.6

Table 10: Speed of MiniCPM-2.4B on different end devices.

Translation

Prompt: Translate this sentence into French: "I am a freshman on Chinese, do you know how this sentence is translated: Python" (How to create a simple web crawler in Python?)

MiniCPM-1.2B:

Je suis un homme nouveau en chinois, vous êtes-vous au courant de la manière dont cette phrase est traduite : Comment créer un petit scraper web simple à Python ?

MiniCPM-2.4B-DPO:

Je suis un nouveau-né en chinois, sais-tu comment on crée un simple web crawler en Python ? Translation: "Je suis un nouveau-né en chinois, sais-tu comment on crée un simple web crawler en Python ?"

Figure 18: Examples on translation. We notice that MiniCPM-2.4B-DPO performs better in translating the technical part, but both models are unnatural in expressing "just starting to learn Chinese.". However, both models successfully understand the instruction with traps and generate French despite we do not include French corpus intentionally.

Math and Reasoning

Prompt: 15-25-12+34=

(If in the following equation, minus signs represent addition, and plus signs represent subtraction, give the result of the calculation: 15-25-12+34=)

MiniCPM-1.2B:

$$15 + 25 + 12 - 34$$

$$15 + 25 = 40$$

$$40 + 12 = 52$$

$$52 - 34 = 18$$

18
(If the minus sign represents a plus sign, then we can rewrite the equation as: 15 + 25 + 12 - 34.
First, calculate the sum of the first two numbers: 15 + 25 = 40.
Then, calculate the sum of the first three numbers: 40 + 12 = 52.
Finally, calculate the difference between the last number and the sum of the first three numbers: 52 - 34 = 18.
Therefore, the result of the equation is 18.)

MiniCPM-2.4B-DPO:

$$15+25+12-34$$

$$(15+25)+12-34=40+12-34=52-34=18$$

18
(If minus signs all represent addition, and plus signs actually represent subtraction, then the equation can be re-expressed as:
15+25+12-34.
Now we can calculate according to the order of addition and subtraction:
(15+25)+12-34 = 40+12-34 = 52-34 = 18
So, the final result of the calculation is 18.)

Figure 19: Examples on math and reasoning. Both models are successful in symbolic substitution and math calculation.

Instruction Following

Prompt:
(Writing an acrostic poem, with the hidden message "Good luck in the Year of the Dragon.")

MiniCPM-1.2B:

(The spring water in the dragon's pool rises,
The sun rises at the phoenix gate.
When will good fortune arrive,
Peace and prosperity are hidden in signs.)

MiniCPM-2.4B-DPO:

(Dragons soar for thousands of miles, their energy like a rainbow,
As the new year begins, joyous occasions abound.
Auspicious days are worth enjoying together,
Good fortune and happiness bring rosy smiles.)

Figure 20: Examples on instruction following. MiniCPM-2.4B-DPO successfully follows the instructions and generates a poem with the correct tonal pattern and the first character of each sentence. However, MiniCPM-1.2B only generates the correct tonal pattern.

Emoji

Prompt: json key emoji value emoji 10

(Please give me a JSON object where each key is an emoji and each value is the meaning of that emoji, providing around 10 examples.)

MiniCPM-1.2B:

10 emoji JSON

```
{
  "😊": " ",
  "😂": " ",
  "😍": " ",
  "🥰": " ",
  "😘": " ",
  "🥳": " ",
  "😎": " ",
  "🤩": " ",
  "🥳": " ",
  "🙏": " ",
  "💩": " "
}
```

JSON
(Of course, this is a JSON file containing around 10 emojis and their meanings:

```
{
  "😊": "smiling",
  "😂": "laughing",
  "😍": "amazing",
  "😘": "kissing",
  "🤩": "mischief",
  "😢": "disappointment",
  "🤔": "thinking",
  "🤑": "money",
  "🙏": "help",
  "💩": "rubbish"
}
```

Hope you found this JSON useful!)

MiniCPM-2.4B-DPO:

10 emoji JSON

```
{
  "😊": " ",
  "😡": " ",
  "😂": " ",
  "🤣": " ",
  "🥳": " ",
  "😍": " ",
  "🤩": " ",
  "❤️": " ",
  "💡": " ",
  "😊": " "
}
```

JSON
(Of course! Here is a JSON object containing 10 emojis and their corresponding meanings:

```
{
  "😊": "It means happy or satisfied, typically used to express smiling and joy.",
  "😡": "It means anger or dissatisfaction, typically used to express intense emotions.",
  "😂": "It means laughing or happy, typically used to express laughter and joy.",
  "🤣": "It means funny or awkward, typically used to express humorous situations or awkwardness.",
  "🥳": "It means surprise or shock, typically used to express a strong reaction to an event or situation.",
  "😍": "It means disappointment or discouragement, typically used to express a loss of interest or confidence in something or someone.",
  "❤️": "It means heartache or sadness, typically used to express intense feelings of pain caused by something or someone.",
  "💡": "It means surprise or excitement, typically used to express the emotion of discovery or finding something or someone.",
  "😊": "It means cool or stylish, typically used to express a confident, independent, and trendy attitude.",
  "🤩": "It means like or appreciate, typically used to express affection or admiration for something or someone."
}
```

I hope this JSON object meets your needs! If you have any questions, please feel free to let me know.)

Figure 21: Examples on emoji. Both models understand emojis and structured data well, and accurately control the number of items implicitly. The DPO model tends to generate more words.